



Dysferlin deficiency alters lipid metabolism and remodels the skeletal muscle lipidome in mice^S

Vanessa R. Haynes,* Stacey N. Keenan,* Jackie Bayliss,* Erin M. Lloyd,[†] Peter J. Meikle,[§] Miranda D. Grounds,^{1,†} and Matthew J. Watt^{1,*}

Department of Physiology,* Faculty of Medicine, Dentistry and Health Sciences, University of Melbourne, Melbourne, Australia; School of Human Sciences,[†] University of Western Australia, Perth, Australia; and Metabolomics Laboratory,[§] Baker Heart Institute, Melbourne, Australia

Abstract Defects in the gene coding for dysferlin, a membrane-associated protein, affect many tissues, including skeletal muscles, with a resultant myopathy called dysferlinopathy. Dysferlinopathy manifests postgrowth with a progressive loss of skeletal muscle function, early intramyocellular lipid accumulation, and a striking later replacement of selective muscles by adipocytes. To better understand the changes underpinning this disease, we assessed whole-body energy homeostasis, skeletal muscle fatty acid metabolism, lipolysis in adipose tissue, and the skeletal muscle lipidome using young adult dysferlin-deficient male BLAJ mice and age-matched C57Bl/6J WT mice. BLAJ mice had increased lean mass and reduced fat mass associated with increased physical activity and increased adipose tissue lipolysis. Skeletal muscle fatty acid metabolism was remodeled in BLAJ mice, characterized by a partitioning of fatty acids toward storage rather than oxidation. Lipidomic analysis identified marked changes in almost all lipid classes examined in the skeletal muscle of BLAJ mice, including sphingolipids, phospholipids, cholesterol, and most glycerolipids but, surprisingly, not triacylglycerol. These observations indicate that an early manifestation of dysferlin deficiency is the reprogramming of skeletal muscle and adipose tissue lipid metabolism, which is likely to contribute to the progressive adverse histopathology in dysferlinopathies.—Haynes, V. R., S. N. Keenan, J. Bayliss, E. M. Lloyd, P. J. Meikle, M. D. Grounds, and M. J. Watt. **Dysferlin deficiency alters lipid metabolism and remodels the skeletal muscle lipidome in mice.** *J. Lipid Res.* 2019. 60: 1350–1364.

Supplementary key words lipolysis • fatty acid metabolism • insulin resistance • adipose tissue • lipidomics • BLAJ mice • dysferlin

Dysferlinopathies are a group of autosomal recessive rare muscular dystrophies that result from mutations in the dysferlin gene, first described in 1998 (1), and character-

ized by the onset of muscle weakness and loss of function usually in the late teens and with slow progression (2). Dysferlinopathies include limb-girdle muscular dystrophy type 2B and Miyoshi myopathy, with the proximal and distal limb-girdle muscles being the main muscles affected (2–4). Mouse models of dysferlinopathy harboring dysferlin deficiency or deletion (5–8) consistently have a late onset of dystropathology, by about 8 months of age, with pronounced replacement of myofibers by adipocytes (9).

Dysferlin is a member of a large ferlin family of transmembrane proteins that are involved in protein vesicle trafficking and fusion (10), with dysferlin initially attracting attention due to its role in the resealing of experimentally damaged sarcolemma (11–13). Dysferlin is localized in intracellular membranes of skeletal muscles such as T-tubules and sarcoplasmic reticulum (14), plays a role in T-tubule formation (15), and appears to be involved in calcium homeostasis related to excitation-contraction coupling (16–18). Dysferlin is highly expressed in skeletal myofibers but is also present in many other tissues (19) and cells, including adipocytes (20), macrophages (21), and endothelium (22).

Two striking features of human and mouse dysferlin-deficient muscles are the accumulation of many lipid droplets within myofibers and, at a later age, the apparent replacement of myofibers with extramyocellular adipocytes (9, 15). Histopathology is not evident in young mice aged ~3 months but is pronounced by 8–12 months in some muscles, including psoas and quadriceps, with increasing severity by 19 months (23). Indeed, in older *Dysf*-deficient A/J mice, 20% to 40% of the myofibers in quadriceps and psoas muscles are replaced by adipocytes (15, 23). In humans,

This work was supported by infrastructure and technical assistance from the Melbourne Mouse Metabolic Phenotyping Platform at the University of Melbourne, Muscular Dystrophy Association Grant MDA418743 (M.D.G., M.J.W.), National Health and Medical Research Council of Australia Senior Research Fellowships APP1077703 and APP1042095 (M.J.W., P.J.M.), and an Australian government research training program scholarship (E.L.).

Manuscript received 1 November 2018 and in revised form 14 May 2019.

Published, JLR Papers in Press, June 15, 2019

DOI <https://doi.org/10.1194/jlr.M090845>

Abbreviations: ATGL, adipose triglyceride lipase; DG, diacylglycerol; MARP, Monash Animal Research Platform; PC, phosphatidylcholine; PE, phosphatidylethanolamine; RER, respiratory exchange ratio; RT, room temperature; TG, triacylglycerol; VCO₂, carbon dioxide production; VO₂, oxygen consumption.

¹To whom correspondence should be addressed.

e-mail: miranda.grounds@uwa.edu.au (M.D.G.); matt.watt@

unimelb.edu.au (M.J.W.)

^SThe online version of this article (available at <http://www.jlr.org>) contains a supplement.

Copyright © 2019 Haynes et al. Published under exclusive license by The American Society for Biochemistry and Molecular Biology, Inc.

This article is available online at <http://www.jlr.org>

MRI analysis shows extensive muscle replacement by adipocytes and that the soleus, which is a slow postural muscle in the lower leg, is one of the earliest muscles to undergo this extensive remodeling (4). While a relatively very low level of myonecrosis is seen in dysferlin human and mouse muscles (9, 24), the striking features are myofiber atrophy (25), associated with degeneration, loss of myofilaments, and some form of autolysis/proteolysis (9, 26), that may account for the later major myofiber loss associated with replacement by adipocytes.

To date, there is little understanding of the factors contributing to the marked intramyocellular lipid accumulation in the muscles of young mice and their possible contribution to the later progressive replacement of muscles by adipocytes in dysferlinopathic muscles (3). This study focuses on systemic and local changes that might contribute to the intramyocellular lipid accumulation in *Dysf*-deficient BLAJ mice by investigating whole-body energy homeostasis, adipose tissue lipolysis, skeletal muscle lipid metabolism, and the skeletal muscle lipidome. Studies were performed in young adult male BLAJ and WT mice to ascertain whether changes in lipid metabolism within BLAJ myofibers are present before the later onset of marked changes in histopathology and complications of adipocyte accumulation.

MATERIALS AND METHODS

Dysferlin-deficient mouse model

BLAJ mice (B6.A-dysf^{fl^{prmal}}/GeneJ) were obtained from the Animal Resources Centre (Murdoch, Australia). Control C57Bl/6J mice were obtained from Monash Animal Research Platform (MARF; Melbourne, Australia). Mice were housed on a 12-h light/dark cycle with free access to a standard rodent chow diet (9% total digestible energy from lipids, 12.8 MJ/kg; Barastoc irradiated mice cubes; Ridley Agri Products, Melbourne, Australia) and drinking water. Experimental protocols were approved by the MARF Animal Ethics Committee (MARF/2017/012) and conformed to the National Health and Medical Research Council of Australia code of practice. Whole-body metabolic phenotyping assessments were conducted in male mice aged 12–16 weeks. Tissues were dissected from 18-week-old mice for ex vivo metabolic assessments and lipidomic analysis.

Body composition

An MRI (EchoMRI 3-in-1) was used to assess lean and fat mass in conscious mice. Mouse tissues were weighed at the time of killing in mice aged 18 weeks. To measure the liver wet to dry ratio, ~100 mg fresh liver tissue was weighed, dehydrated overnight under vacuum at 30°C, and then weighed again. Tissue triacylglycerol (TG) content was assessed after Folch lipid extraction and biochemical assessment (Roche Diagnostics, Basel, Switzerland).

Liver glycogen content

Approximately 20 mg liver was digested in 200 μ l 1 M KOH at 70°C. The glycogen was precipitated by the addition of 75 μ l saturated Na₂SO₄ and 1.725 ml 95% ethanol. Samples were mixed and centrifuged at 1,500 g for 10 min to pellet the glycogen. The pellet was resuspended in 200 μ l ddH₂O, and the glycogen was again pelleted by adding 1.8 ml 95% ethanol, mixed, and spun at 1,500 g for 10 min. The pellet was dried and resuspended

in 300 μ l 0.3 mg/ml amyloglucosidase in 0.25 M acetate buffer, pH 4.75, and incubated overnight at 37°C to ensure the full digestion of glycogen into glycosyl units. The glucose concentrations were determined using a glucose oxidase kit (Thermo Fisher Scientific, Waltham, MA).

Respiration, energy expenditure, physical activity, and food intake

Gas-exchange indirect calorimetry uses measurements of an animal's oxygen consumption (VO₂) and carbon dioxide production (VCO₂) to calculate energy expenditure. Mice were housed individually for 3 days in airtight calorimetry chambers connected to a multiplexed gas sensor unit to assess VO₂ and VCO₂ (Promethion; Sable Systems International, North Las Vegas, NV). The respiratory exchange ratio (RER) was calculated as VCO₂/VO₂. Energy expenditure was calculated from VO₂ and RER using Weir constants and normalized to lean mass. Food and water intake were recorded every 15 min. Physical activity was recorded via beam breaks (BXYZ Beambreak Activity Monitor; Sable Systems International).

Food intake and plasma lipids

Mice were fasted overnight from 4:00 PM to 8:00 AM. Food was placed in the cage, and ad libitum food intake was assessed for 90 min. In separate experiments, mice were fasted for 6 h (7:00 AM to 1:00 PM), and then blood was collected from the tail tip before and after a 60 min period of ad libitum refeeding. Plasma NEFAs (Wako, Osaka, Japan), glycerol (Sigma-Aldrich, St. Louis, MO), and TGs (Roche Diagnostics) were measured biochemically. To measure TG secretion, mice were fasted for 4 h (7:00 AM to 11:00 AM), and a plasma sample was collected. Mice were injected intraperitoneally with 1 mg poloxamer 407 (LPL inhibitor; Sigma-Aldrich) per gram of body mass in saline. Plasma was collected at 60 and 120 min, and TG was measured biochemically.

Glucose metabolism and blood chemistry

An oral glucose tolerance test was used to assess glucose tolerance in mice. Mice were fasted for 4 h from 7:00 AM to 11:00 AM. Blood glucose was measured before and after a bolus of glucose was administered via oral gavage [200 μ l 25% D-glucose (w/v) dissolved in water]. Blood was collected at 0, 15, and 30 min, and plasma insulin levels were assessed using ELISA (Crystal Chem; Downers Grove, IL). To assess whole-body insulin sensitivity, mice were fasted for 4 h from 7:00 AM to 11:00 AM and subjected to an intraperitoneal insulin tolerance test. Blood glucose was measured before and after an intraperitoneal injection of 0.75 insulin units/kg body mass.

To determine the phosphorylation of specific insulin-signaling proteins, liver was collected from mice under insulin-stimulated conditions (0.75 units/kg body weight; intraperitoneal injection 10 min before being culled). Tissue was homogenized in ice-cold RIPA buffer [65 mM Tris HCl, 150 mM NaCl, 1% NP-40 (v/v), 0.5% sodium deoxycholate (v/v), 0.1% SDS (v/v), and 1% glycerol (v/v)] with 1 mM DTT, protease (Complete Protease Inhibitor Cocktail; Roche Diagnostics), and phosphatase (PhosSTOP Phosphatase Inhibitor Cocktail; Roche Diagnostics) inhibitors using a tissue lyser (TissueLyser LT; Qiagen, Hilden, Germany). The samples were centrifuged, and 15 μ g liver protein was denatured and resolved by SDS-PAGE. Stain-free images were collected after the transfer to confirm equal protein loading (ChemiDoc MP and ImageLab version 4.1; Bio-Rad Laboratories, Gladesville, Australia). Membranes were blocked with 5% BSA in TBS-T for 1 h to reduce nonspecific binding and incubated with primary antibodies (1:1,000) overnight at 4°C. Primary antibodies used were phospho Akt (Ser473), total Akt, and total IRS (Cell Signaling, Danvers, MA) and phospho IRS (Tyr 612; Sigma-Aldrich).

Membranes were washed in TBS-T and incubated with their corresponding horseradish peroxidase-conjugated secondary antibodies for 2 h. The membranes were washed again, visualized, and imaged using Clarity Western ECL substrate (Bio-Rad Laboratories) and the ChemiDoc MP system. Protein density was quantified using ImageLab version 4.1.

Tissue metabolism ex vivo

To assess fatty acid metabolism in tissues ex vivo, 18-week-old mice were anesthetized by isoflurane inhalation (1.5%; Baxter Healthcare, Toongabbie, Australia). The soleus muscle and a liver slice (~20 mg) were dissected, and tissues were weighed and then incubated at 37°C for 2.5 h in pre-gassed (95% O₂, 5% CO₂) DMEM containing 5 mM glucose and 0.5 mM oleic acid and 1 μCi/ml [1-¹⁴C]oleic acid conjugated to 1% (w/v) BSA. Released CO₂ was captured and radioactivity determined by liquid scintillation counting (LS6500; Beckman Coulter, Indianapolis, IN) to assess complete fatty acid oxidation. Tissues were washed in PBS (Thermo Fisher Scientific), homogenized manually in 2:1 chloroform-methanol, and centrifuged at 1,000 g for 10 min to separate the organic and aqueous phases. ¹⁴C within the aqueous phase was measured to assess the acid-soluble metabolites, which represents incomplete fatty acid oxidation (S6500; Beckman Coulter). The organic phase was transferred to a 12 × 75 mm glass tube and dried under nitrogen gas at 40°C. The dried lipids were reconstituted in 50 μl chloroform-methanol (2:1) containing 1.75 mg/ml glyceryl tripalmitate (TG; TS5888; Sigma-Aldrich) to facilitate the visualization of lipid bands. Samples were spotted onto 250 μm glass-backed silica gel plates (20 × 20 cm; Analtech, Newark, DE) using a 100 μl TLC syringe (1710SN; Hamilton, Bonaduz, Switzerland). A three-step TLC method was used to separate the polar and nonpolar lipids. The plate was first developed in chloroform-methanol-water (65:25:4) until the solvent reached 50% of the plate length. The plate was then developed in hexane-diethyl ether-acetic acid (75:35:1) until the solvent reached 90% of the plate height, and this second solvent step was repeated. Plates were air dried and sprayed with 2',7'-dichlorofluorescein dye (0.02% w/v in ethanol; Sigma-Aldrich), lipid bands were visualized under UV light and scraped into scintillation vials with 5 ml scintillation cocktail (Ultima Gold; Perkin Elmer, Akron, OH), and ¹⁴C was counted. The incorporation of ¹⁴C-labeled fatty acid into TGs and the remainder of the plate were then measured.

To measure lipolysis, ~40 mg pieces of epididymal white adipose tissue and inguinal white adipose tissue were dissected from anesthetized mice and incubated at 37°C for 2 h in Krebs buffer containing 2% BSA and 5 mM glucose (spontaneous) or with the addition of 1 μM isoproterenol (stimulated), which is a pan β-adrenergic agonist. Free fatty acid release into the medium (i.e., lipolysis) was determined biochemically (Wako).

Lipidomic analysis

Snap-frozen samples of quadriceps (~30 mg) were homogenized in 900 μl soap-free RIPA buffer, and total protein was determined by BSA assay (Pierce 660 nm Protein Assay; Thermo Fisher Scientific). A 50 μl aliquot of muscle homogenate was combined with 15 μl internal standard mix and 1,000 μl chloroform-methanol (2:1) and then mixed. A water blank, an internal standards blank, and an unextracted blank were also included. Samples were mixed with a rotary mixer for 10 min, sonicated at room temperature (RT) for 30 min, and then allowed to stand at RT for 20 min. Samples were centrifuged at 16,000 g for 10 min at RT. The supernatant was transferred to wells of a 96-well plate (0.5 ml polypropylene) and dried under nitrogen stream at 40°C. Samples were reconstituted in 50 μl water-saturated butanol and sonicated for 10 min at RT, and then 50 μl 10 mM ammonium formate in methanol was added to each sample. Extracts were centrifuged

at 3,000 g for 5 min. The supernatant was transferred into 0.2 ml microinserts in 32 × 11.6 mm glass vials with Teflon insert caps. Analysis was performed by electrospray ionization-tandem mass spectrometry. An Agilent 1200 liquid chromatography system was used with a Zorbax C18, 1.8 μm, 50 × 2.1 mm column (Agilent Technologies, Santa Clara, CA). The columns were heated to 50°C; the autosampler was heated to 25°C. Solvents A and B were composed of tetrahydrofuran-methanol-water in the ratio 30:20:50 and 75:20:5, respectively, both containing 10 mM NH₄COOH. To determine TG and diacylglycerol (DG) species, 1 μl of injection was separated using isocratic flow (100 μl/min) of 85% solvent B over 6 min. For all other lipid species analysis, 5 μl of injection was separated under gradient conditions (300 μl/min) 0% to 100% solvent B over 8 min, 2.5 min at 100% B, a return to 0% B over 0.5 min, and then 10.5 min at 0%. The mass spectrometer used was an Applied Biosystems API 4000 Q/TRAP with a turbo ionspray source (350°C) and Analyst 1.5 data system. Quantification of individual lipid species was performed using scheduled multiple reaction monitoring in positive ion mode and Multiquant version 1.2. Lipid concentrations were calculated by relating the peak area of each species to the peak area of the corresponding internal standard. The total lipid concentration of each class was calculated by summing the individual lipid species. Data presented have been normalized to total protein concentration, but results were similar when data were normalized to initial tissue weight or to total phosphatidylcholine (PC).

Analysis of gene expression

Mixed quadriceps muscle was homogenized in TRI reagent (1 ml per 50 mg tissue; Sigma-Aldrich). Total RNA was extracted, and 1 μg mRNA was reverse transcribed (iScript cDNA Synthesis Kit; Bio-Rad Laboratories). Gene products were measured by quantitative real-time PCR (CFX Connect Real-Time PCR Detection System; Bio-Rad Laboratories) using the QuantiNova SYBR Green PCR Kit (Qiagen). Skeletal actin (*Acta1*) was used as a reference gene and did not vary between groups. The relative quantification was calculated using the ΔΔCt method, and values were normalized to WT. Primer sequences are listed in **Table 1**.

Statistical analyses

Data are reported as means ± SEMs. To examine differences between BLAJ and WT mice, data were analyzed with unpaired two-tailed *t*-tests or two-way ANOVA with Bonferroni post hoc testing where appropriate. Statistical significance was determined a priori at *P* < 0.05.

RESULTS

Body composition

The total body mass of 16-week-old *Dysf*-deficient BLAJ mice was not significantly different from age-matched WT control mice (**Fig. 1A**), whereas the body composition was strikingly different. MRI showed that lean mass was increased by 8% and total fat mass was decreased by 69% in BLAJ compared with WT mice (**Fig. 1B, C**). Consistent with the MRI data, the epididymal and subcutaneous adipose depots weighed 71% and 61% less in BLAJ mice compared with WT mice (**Table 2**). There was no significant difference between genotypes for the soleus muscle, extensor digitorum longus muscle, mixed quadriceps muscle, or heart mass (**Table 2**), whereas liver mass was increased by 27% in BLAJ mice (**Table 2**). The increase in liver mass was

TABLE 1. List of genes quantified by PCR

Gene	Encoding Protein	Sequence
<i>Abhd5</i>	1-Acylglycerol-3-phosphate <i>O</i> -acyltransferase (also known as CGI-58)	Forward: 5'-TTGGGTAAAGTCTAGTGCAG Reverse: 5'-TTTTTGAAAGCTGTCTCACC
<i>Arsb</i>	Arylsulfatase B	Forward: 5'-ACACGCCGAGGATTCCGATAC Reverse: 5'-CAAAGACTAATCGGCGCAC
<i>Asah1</i>	<i>N</i> -Acylsphingosine amidohydrolase 1	Forward: 5'-AGGACGTAAGTCTGAGACCCGAA Reverse: 5'-GACAAGAGGCCTTGAGCCTT
<i>Cd36</i>	Cluster of differentiation 36 (also known as fatty acid translocase, FAT/CD36)	Forward: 5'-CATTTCAGGCTCTATCTACG Reverse: 5'-CAATGTCTAGCACACCATAAG
<i>Cerk</i>	Ceramide kinase	Forward: 5'-TGGTCTTGTGGCTTCAAGATT Reverse: 5'-ATGAGGGGAGGCCATAGTCTG
<i>Cpt-1b</i>	Carnitine palmitoyltransferase 1B	Forward: 5'-ACTAACTATGTGAGTGACTGG Reverse: 5'-TGGCATAATAGTTGCTGTTC
<i>Dgat2</i>	Acyl-CoA:diacylglycerol acyltransferase 2	Forward: 5'-GTGGCAATGCTATCATCATC Reverse: 5'-CTGCTGTATACCTCATTCTC
<i>Glb1</i>	Galactosidase, β 1	Forward: 5'-TTCCGGATACCCCGCTTCTA Reverse: 5'-GAAGTCAAGGGCACGTACA
<i>Gpam</i>	Glycerol-3-phosphate acyltransferase 1, mitochondrial (also known as GPAT1)	Forward: 5'-CATTGAGATTCACAAGGGTC Reverse: 5'-GTGAATCAAGGTACTGAAGAC
<i>Hexb</i>	Hexosaminidase B	Forward: 5'-GGTTGGTCCAAAGACTGCCT Reverse: 5'-GACACTAGCGACACCAGCG
<i>Lipe</i>	Hormone-sensitive lipase	Forward: 5'-AACTCCTTCTGCAACTAAG Reverse: 5'-CTTCTTCAAGGTATCTGTGC
<i>Pdk4</i>	Pyruvate dehydrogenase kinase isozyme 4, mitochondrial	Forward: 5'-ACAATCAAGATTTCTGACCG Reverse: 5'-TCTCCTTGAAAATACTTGGC
<i>Pisd</i>	Phosphatidylserine decarboxylase	Forward: 5'-TGTAACACATGCCAACAAGG Reverse: 5'-ATCTTATAAGGTCAGCCCGG
<i>Plin2</i>	Perilipin 2 (also known as adipose differentiation-related protein, ADRP)	Forward: 5'-ATAAGCTCTATGTCTCGTGG Reverse: 5'-GCCTGATCTTGAATGTTCTG
<i>Plin5</i>	Perilipin 5 (also known as lipid storage droplet protein 5, LSDP5)	Forward: 5'-TGTAGTGTGACTACCTGTG Reverse: 5'-ATGTCACCACCATGTCTG
<i>Pnpla2</i>	Patatin-like phospholipase domain containing 2 (also known as adipose ATGL)	Forward: 5'-CAACCTTCGCAATCTCTAC Reverse: 5'-TTCAGTAGGCCATTCCCTC
<i>Ppargc1a</i>	PPARG coactivator 1 α	Forward: 5'-TCCTCTTCAAGATCCTGTTAC Reverse: 5'-CACATACAAGGGAGAATTGC
<i>Ptdss1</i>	Phosphatidylserine synthase 1	Forward: 5'-ATTCTCCCTGTCTACCCTGG Reverse: 5'-TGCATACACTTCCATTCCCT
<i>Sgpl1</i>	Sphingosine phosphate lyase 1	Forward: 5'-ATGTGGATGCTTGTCTGGGG Reverse: 5'-GTCACACCTTTACCCGGAA
<i>Acta1</i>	Skeletal actin	Forward: 5'-TATTCCTTCGTGACCACAGCT Reverse: 5'-CGCGAACGCAGACGCGAGTG

not explained by changes in liver glycogen or TG contents, which were actually lower in BLAJ mice (Table 2). Because dysferlinopathies are associated with the development of edema in skeletal muscle (3), we assessed the wet to dry ratio in livers from mice, but there was no difference between genotypes (WT = 3.31 ± 0.09 ; BLAJ = 3.11 ± 0.22 ; $P = 0.39$; $n = 8/\text{group}$).

Energy homeostasis

Whole-body energy homeostasis was assessed using the Promethion metabolic phenotyping system. Whole-body substrate oxidation was different between genotypes, as shown by a significant increase in the RER in BLAJ mice (Fig. 1D). This demonstrates a preference for carbohydrate oxidation in the BLAJ mice. Daily energy expenditure was not different between genotypes when normalized to lean body mass (Fig. 1E). Daily physical activity was increased in BLAJ mice (Fig. 1F), and daily food intake tended to increase in BLAJ mice, but this did not reach statistical significance (Fig. 1G; $P = 0.052$ by two-way ANOVA; WT = 1.99 ± 0.25 g; BLAJ = 2.81 ± 0.30 g). Consistent with this notion, BLAJ mice consumed ~ 2.1 times more food than WT mice in the 90 min refeeding period after a 16 h fast (Fig. 1H).

Glucose metabolism and blood chemistry

Reductions in fat mass are often associated with improved glycemic control; however, fasting blood glucose and glucose clearance in response to an oral glucose load were not different between the genotypes (Fig. 2A). Notably, plasma insulin levels were increased in BLAJ mice with fasting and glucose administration, indicating the possibility of insulin resistance in this genotype (Fig. 2B). This was not borne out during an insulin tolerance test, which demonstrated no difference in whole-body insulin sensitivity between genotypes (Fig. 2C). In support of these findings, insulin-stimulated phosphorylation of liver IRS-1 T612 and Akt S473 was not different between WT and BLAJ mice (Fig. 2D), and liver glycogen contents were also similar between genotypes (Table 2). Plasma NEFAs, glycerol, and TGs were not different between genotypes under fed or fasted conditions (Fig. 2E, G). Consistent with this latter finding, TG secretion was similar in WT and BLAJ mice (Fig. 2H).

Fatty acid metabolism and lipolysis assessed ex vivo

Dysferlinopathies are characterized by an accumulation of lipid droplets within myofibers, and we hypothesized that this may result from defective skeletal muscle fatty acid metabolism. Accordingly, radiolabeled tracers were used to

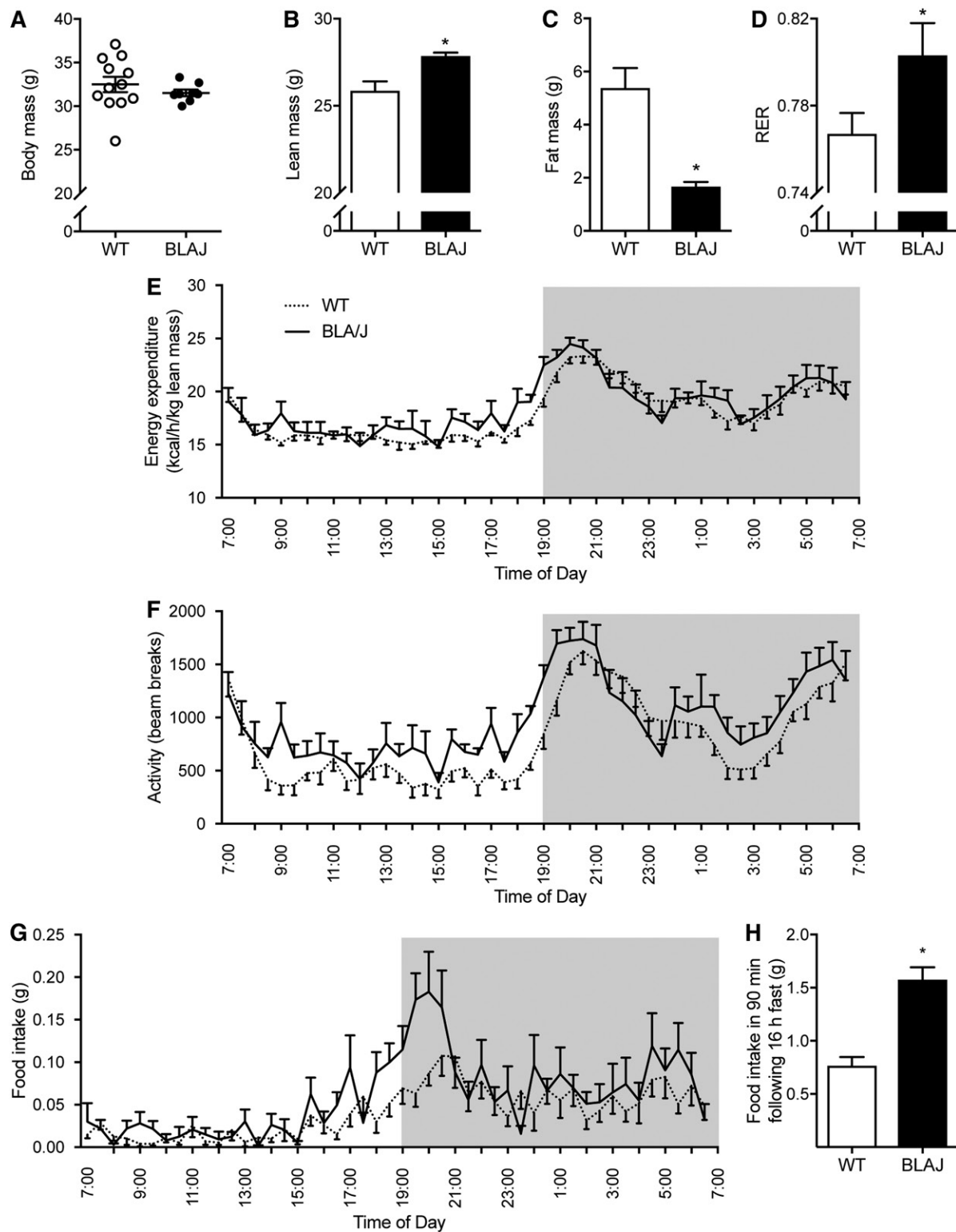


Fig. 1. Body composition and whole-body energy homeostasis. Measurements made in WT and *Dysf*-deficient BLAJ male mice aged 16 weeks. Body mass (A), lean mass (B), and fat mass (C) assessed by MRI. D: RER averaged over 24 h. Energy expenditure (E), physical activity (F), and food intake (G) assessed over 24 h, $n = 12$ WT and $n = 8$ BLAJ mice. H: Food intake in the 90 min after an overnight fast, $n = 6$ WT and $n = 4$ BLAJ mice. Data are means \pm SEMs. * $P < 0.05$ versus WT as assessed by two-tailed unpaired *t*-test (A–D, H). $P < 0.05$ genotype effect as assessed by two-way repeated-measures ANOVA (F).

assess fatty acid uptake, oxidation, and storage into various lipid pools in soleus muscles isolated from young adult mice. Fatty acid uptake tended to be increased in BLAJ compared with WT mice (Fig. 3A; 28% difference; $P =$

0.09), and this was associated with no significant difference in fatty acid oxidation (Fig. 3B), but fatty acid storage into TGs increased markedly in BLAJ compared with WT mice (Fig. 3C). Gene expression analysis was conducted in the

TABLE 2. Tissue mass and muscle TG content in WT and dysferlin-deficient BLAJ mice

Tissue	WT (mg)	BLAJ (mg)
Quadriceps muscle	237 ± 10	244 ± 6
Soleus muscle	13.2 ± 0.5	13.8 ± 0.7
Extensor digitorum longus muscle	14.0 ± 0.5	13.6 ± 1.0
Heart	155 ± 7	167 ± 2
Epididymal adipose tissue	1,320 ± 169	383 ± 37*
Inguinal adipose tissue	900 ± 124	349 ± 44*
Liver	1,370 ± 43	1,550 ± 57*
Quadriceps TG (μmol/g)	52 ± 16	31 ± 8
Liver TG (μmol/g)	48.7 ± 9.2	10.3 ± 2.5*
Liver glycogen (μmol/g)	27.3 ± 2.4	32.1 ± 3.7

Data were obtained from mice aged 18 weeks that had been fasted for 6 h; $n = 12$ WT and 8 BLAJ mice for all analyses except liver mass, where $n = 24$ WT and $n = 18$ BLAJ mice, and liver glycogen, where $n = 8$ WT and $n = 7$ BLAJ mice. Data are means ± SEMs. * $P < 0.05$ genotype effect as assessed by two-tailed unpaired t -test.

mixed quadriceps muscle of the same mice but not the soleus due to a lack of tissue for analysis. Surprisingly, *Cd36*, the gene encoding the key protein that regulates fatty acid uptake, was reduced in BLAJ compared with WT mice, while genes encoding the key proteins that regulate fatty acid oxidation were not different between genotypes (e.g., *Ppargc1a*, *Cpt1b*, *Pdk4*) (Fig. 4D). *Dgat2*, which encodes acyl-CoA:diacylglycerol acyltransferase, the enzyme that catalyzes the final reaction of TG by covalently joining a fatty acyl-CoA and DG, was increased ~4-fold in BLAJ mice. The expression of genes encoding proteins of TG breakdown were generally unchanged, with the exception in BLAJ mice being a marked decrease in *Atgl*, which encodes the rate-limiting TG lipase adipose triglyceride lipase (ATGL), and an increase in *Plin5*, which encodes an important protein regulating TG metabolism (Fig. 3D). In contrast to skeletal muscle, there was a reduction in liver fatty acid uptake and storage in BLAJ compared with WT mice (Fig. 3E–G; Table 2), supporting the notion that the skeletal muscle defects that occur in dysferlinopathies are not necessarily uniform in all tissues.

Aside from changes in skeletal muscle metabolism, it is possible that the accumulation of lipids previously observed within skeletal muscle could be mediated by increased fatty acid delivery. This would not be evident with measures of plasma NEFAs (Fig. 2D) or plasma glycerol (Fig. 2F), which do not directly assess the rate of fatty acid appearance. Accordingly, we assessed lipolysis in various adipose tissue depots isolated from BLAJ and WT mice. Spontaneous lipolysis was increased by 64% and β -adrenergic-stimulated lipolysis was increased by 77% in the subcutaneous inguinal adipose tissue of BLAJ compared with WT mice (Fig. 3H; main effect for genotype by two-way ANOVA, $P < 0.05$). Similar trends were observed in visceral epididymal adipose tissue, with spontaneous and β -adrenergic-stimulated lipolysis increased by 88% and 27% in BLAJ compared with WT mice, although this did not reach statistical significance when assessed by two-way ANOVA ($P = 0.14$; Fig. 3I).

Skeletal muscle lipidome

While lipid accumulation is a defining feature of dysferlinopathies, this broad description does not provide infor-

mation on the diverse and complex range of lipids that serve a wide array of structural and signaling roles in skeletal muscle. Hence, we next assessed the lipidome of quadriceps muscles from BLAJ and WT mice using electrospray ionization-tandem mass spectrometry to uncover potential relationships between lipid changes and dysferlinopathies. The abundance of each lipid class was expressed as absolute units relative to protein mass (Fig. 4A–D) and the relative differences between genotypes as a percentage change in BLAJ relative to WT (Fig. 4F). Surprisingly, TG levels were not significantly different between genotypes in these young adult mice (Fig. 4C), and this was confirmed by independent analysis using a Folch extraction and TG assessment by biochemical enzymatic spectrophotometric assay (Table 2). This finding differs from previous observations of increased Oil Red O staining of neutral lipids in *Dysf*-deficient skeletal muscle from older mice and humans (9, 15). In contrast with TG, total levels of sphingolipids (94%), cholesterol (80%), cholesteryl esters (183%), and DG (93%) were increased in BLAJ quadriceps, while there were no differences between genotypes for PC, phosphatidylethanolamine (PE), or phosphatidylinositol (Fig. 4A–F; supplemental Tables S1–S4). The PC-PE ratio was similar between genotypes (Fig. 4E). In the sphingolipid class, several subtypes were increased in BLAJ muscles, including sphingomyelin (82%), dihexosylceramide (230%), trihexosylceramide (295%), and GM3 gangliosides (111%) (Fig. 4A, F).

Consistent with the analysis of total lipid content, there were numerous lipid species within each lipid class that were significantly more abundant in the BLAJ skeletal muscle. The complete list is summarized in supplemental Table S1. Of note, individual sphingolipid species with C16:0 side chains were significantly increased (including ceramide, dihydroceramide, monohexosylceramide, dihexosylceramide, trihexosylceramide, ganglioside, and sphingomyelin), and interestingly, there was also accumulation of various sphingolipid species with C24:0 and C24:1 fatty acids (Fig. 5A–F).

An examination of the fatty acid composition of TG, DG, and PC lipid classes revealed subtle differences between WT and BLAJ quadriceps (Fig. 6A–E). Most notable was the general decrease in very-long-chain polyunsaturated fatty acids in PC with concomitant increases in all C18 fatty acids (i.e., stearate, oleate, and linoleate).

Evidence of molecular remodeling of lipidome

In light of the marked changes in the muscle lipidome, we asked whether there was molecular remodeling of lipid metabolism genes in BLAJ mice. Genes that encode regulatory proteins of sphingolipid metabolism were prioritized. There was a marked (>3-fold) increase in mRNA expression of *Glb1*, *Hexb*, *Cerk*, *Arsb*, *Asah1*, and *Sgpl1* genes that encode proteins that catalyze various and diverse reactions of sphingolipid metabolism (Fig. 7A, B). We also examined the expression of *Ptdss1*, which encodes the protein that catalyzes the formation of phosphatidylserine from either PC or PE, and *Pisd*, which catalyzes the conversion of phosphatidylserine to PE: *Ptdss1* tended ($P = 0.10$) to increase, and *Pisd* was significantly increased in BLAJ (~3-fold) compared with WT mice (Fig. 7A).

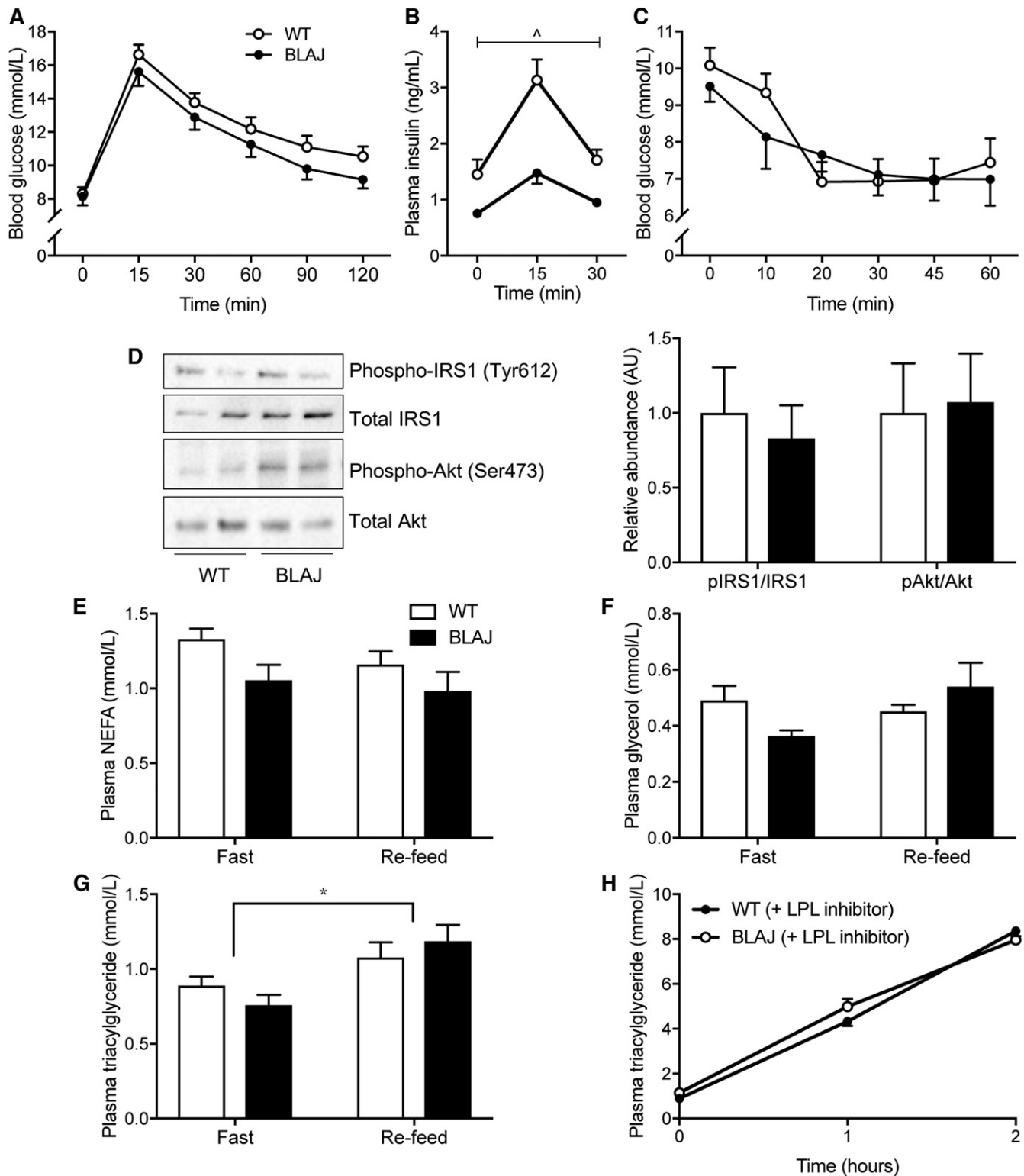


Fig. 2. Glucose metabolism and blood lipids. Measurements made in WT and *Dysf*-deficient BLAJ mice aged 13 weeks. **A:** Blood glucose before and during an oral glucose tolerance test. **B:** Plasma insulin levels assessed before and after oral glucose administration. **C:** Blood glucose levels before and during an intraperitoneal insulin tolerance test, $n = 12$ WT and $n = 8$ BLAJ mice. **D:** Insulin-stimulated phosphorylation of Akt (Ser473) to total Akt and phosphorylation of IRS1 (Tyr 612) to total IRS1 in liver homogenates. The blot is representative of $n = 7$ WT mice and $n = 7$ BLAJ mice. **E–G:** Fasting and refeed plasma NEFA, glycerol, and TG levels, respectively, $n = 8$ WT and 8 BLAJ mice. **H:** Plasma TG during the TG secretion test, $n = 8$ WT and 8 BLAJ mice. Data are means \pm SEMs. $^{\wedge}P < 0.05$ genotype effect as assessed by two-way repeated-measures ANOVA (**B**); $*P < 0.05$ feeding effect as assessed by two-way ANOVA (**G**). AU, arbitrary unit; IRS1, insulin receptor substrate 1.

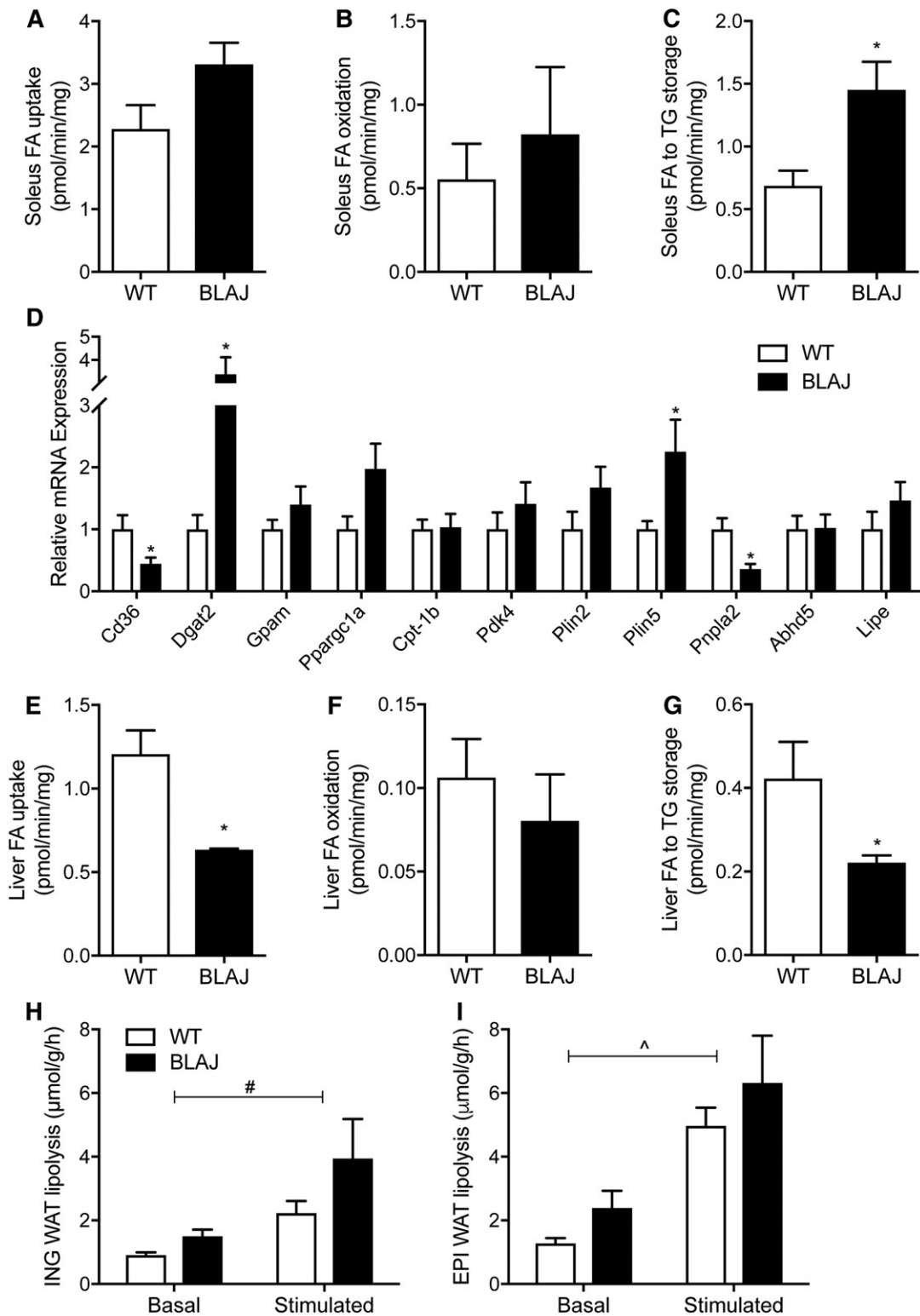


Fig. 3. Lipid metabolism in isolated tissues. Skeletal muscle, liver, and adipose tissues were excised from anesthetized mice, and metabolism was assessed ex vivo. Soleus muscle fatty acid (A) uptake, (B) oxidation, and (C) esterification to TG, $n = 6$ WT and $n = 4$ BLAJ mice. D: Expression of lipid metabolism genes in the quadriceps muscle, $n = 8$ WT and $n = 8$ BLAJ mice. Liver fatty acid (E) uptake, (F) oxidation, and (G) esterification to TG, $n = 6$ WT and $n = 4$ BLAJ mice. Basal and β -adrenergic-stimulated lipolysis was assessed by measuring free fatty acid release from (H) inguinal and (I) epididymal adipose tissues, $n = 12$ WT and $n = 8$ BLAJ. Data are means \pm SEMs. * $P < 0.05$ versus WT as assessed by two-tailed unpaired t -test; # $P < 0.05$ genotype effect and ^ $P < 0.05$ stimulation effect as assessed by two-way repeated-measures ANOVA (H, I). EPI, epididymal; ING, inguinal; WAT, white adipose tissue.

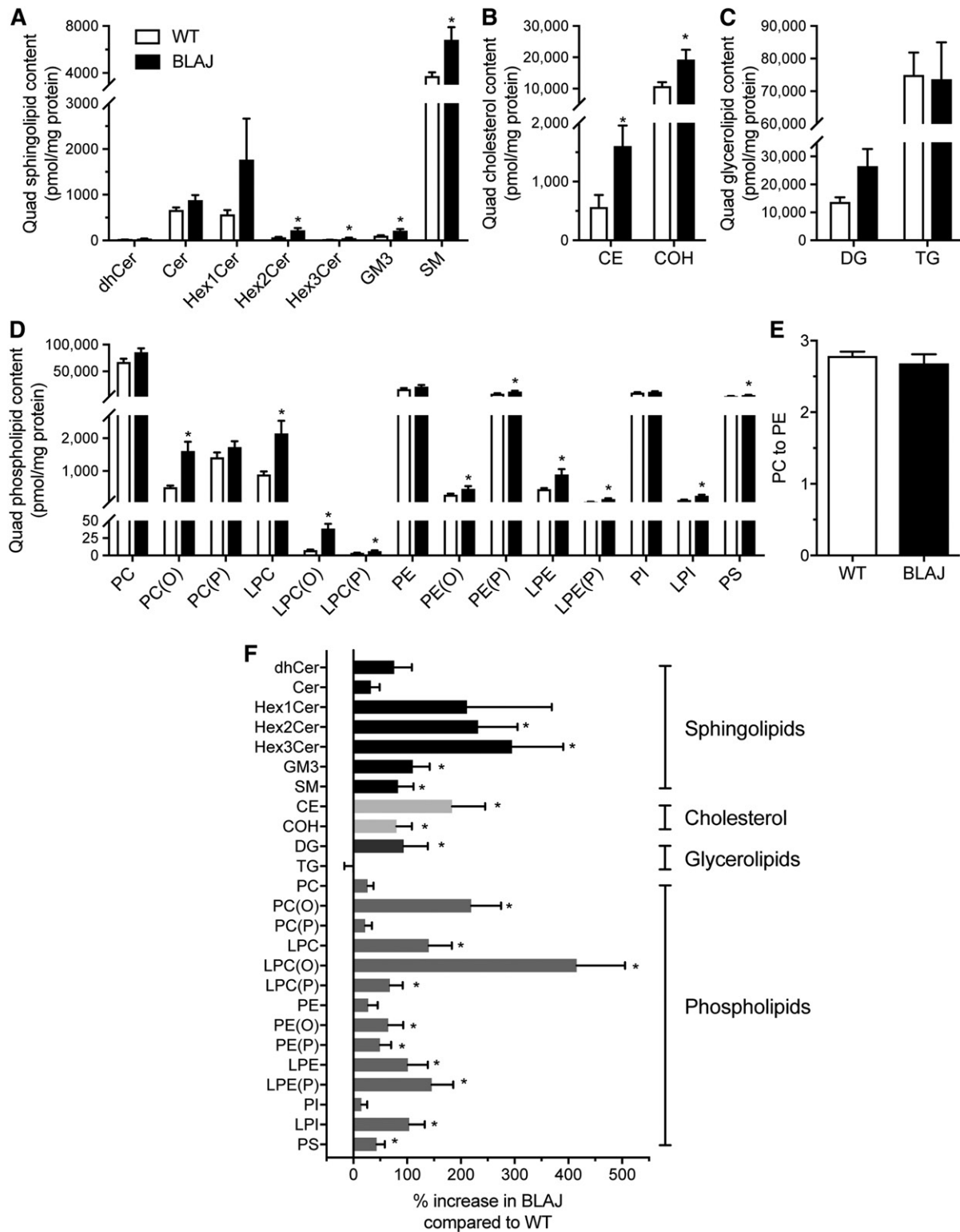


Fig. 4. Skeletal muscle lipidome. Sphingolipid (A), cholesterol (B), glycerolipid (C), and phospholipid (D) content in the quadriceps of WT (white bar) and BLAJ (black bar) mice presented as absolute units relative to protein mass. E: PC:PE ratio. F: Abundance of the lipid classes/subclasses for BLAJ muscles expressed as a percentage change relative to WT. CE, cholesteryl ester; Cer, ceramide; COH, cholesterol; dhCer, dihydroceramide; GM3, G_{M3} ganglioside; Hex1Cer, monohexosylceramide; Hex2Cer, dihexosylceramide; Hex3Cer, trihexosylceramide; LPC, lysophosphatidylcholine; LPC(O), lysoalkylphosphatidylcholine; LPC(P), lysoalkenylphosphatidylcholine; LPE, lysophosphatidylethanolamine; LPE(P), lysoalkenylphosphatidylethanolamine; LPI, lysophosphatidylinositol; PC(O), alkylphosphatidylcholine; PC(P), alkenylphosphatidylcholine; PE(O), alkylphosphatidylethanolamine; PE(P), alkenylphosphatidylethanolamine; PI, phosphatidylinositol; PS, phosphatidylserine. Data are means \pm SEMs, $n = 8$ WT and $n = 8$ BLAJ mice. * $P < 0.05$ versus WT as assessed by two-tailed unpaired t -test.

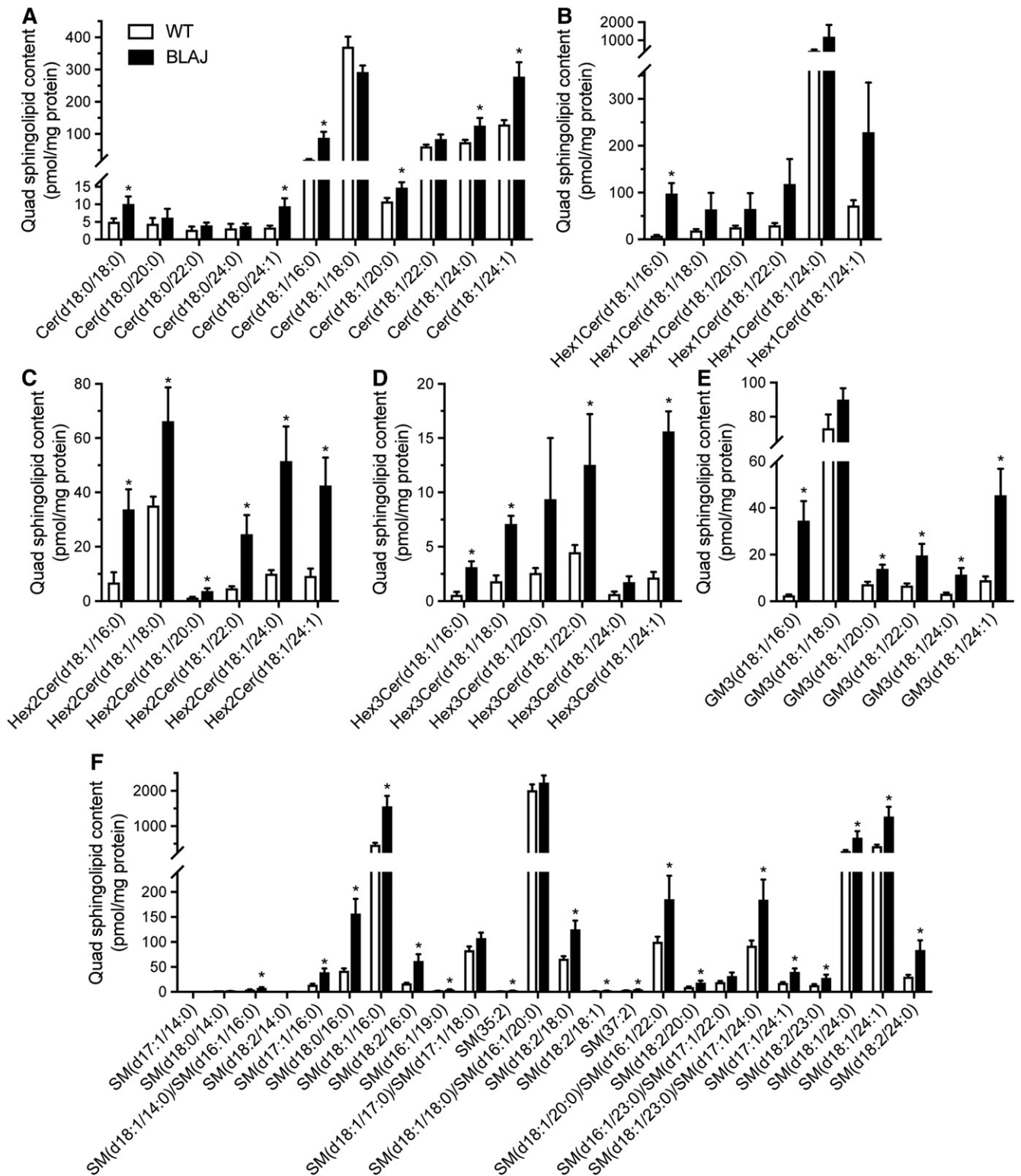


Fig. 5. Skeletal muscle sphingolipid species. Lipid abundance in the quadriceps of WT (white bar) and BLAJ (black bar) mice presented as absolute units relative to protein mass. A: Cer. B: Hex1Cer. C: Hex2Cer. D: Hex3Cer. E: GM3. F: SM. Data are means \pm SEMs, $n = 12$ WT and $n = 8$ BLAJ mice. * $P < 0.05$ as assessed by two-tailed unpaired t -test. Cer, ceramide; GM3, G_{M3} ganglioside; Hex1Cer, monohexosylceramide; Hex2Cer, dihexosylceramide; Hex3Cer, trihexosylceramide.

DISCUSSION

Dysferlinopathies are characterized by pronounced lipid droplet accumulation within myofibers; however, the processes mediating this pathology remain unre-

solved. In this detailed metabolic and lipidomic study of young adult *Dysf*-deficient BLAJ mice, we investigated *Dysf*-deficient skeletal muscle before the onset of conspicuous histopathological complications. With this model, we showed that dysferlin deficiency increases fatty acid

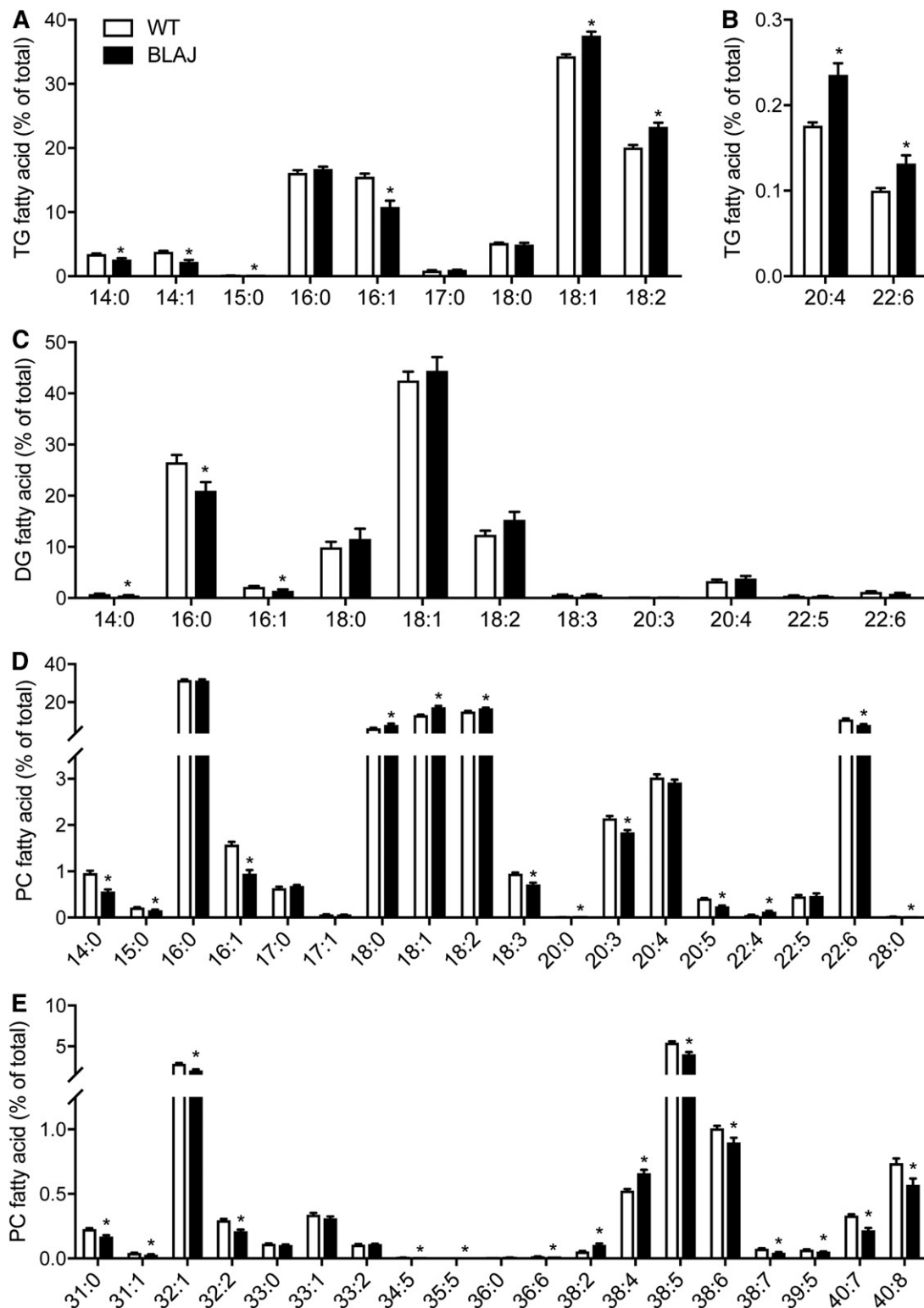


Fig. 6. Fatty acid composition of quadriceps muscle lipids in WT and BLAJ mice. Fatty acid composition (A) of quadriceps muscle in TG (A, B), DG (C), and PC (D, E) are shown as the percentage of total fatty acid within respective lipid classes. Data are means \pm SEMs, $n = 12$ WT and $n = 8$ BLAJ mice. * $P < 0.05$ versus WT as assessed by two-tailed unpaired t -test.

uptake and storage in skeletal muscle, increases lipolysis in white adipose tissue, and alters the expression of genes encoding proteins regulating lipid metabolism. Together, these results implicate these processes as important de-

terminants of the complex remodeling of the skeletal muscle lipidome that is highlighted by the accumulation of many phospholipid, sphingolipid, and cholesterol species.

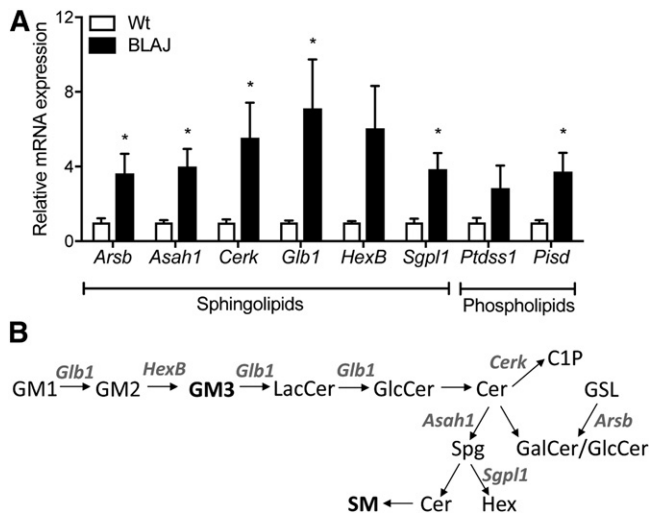


Fig. 7. Genes encoding regulatory proteins of sphingolipid and phospholipid metabolism. A: Expression of key sphingolipid regulatory genes *Glb1*, *Hexb*, *Cerk*, *Arsb*, *Asah1*, and *Sgpl1* and phospholipid regulatory genes *Ptdss1* and *Pisd*. B: Flowchart describing the observed sphingolipid molecular remodeling. Cer, ceramide; C1P, ceramide-1-phosphate; GalCer, galactosylceramide; GlcCer, glucosylceramide; GM1, monosialotetrahexosylganglioside; GM2, G_{M2} ganglioside; GM3, G_{M3} ganglioside; GSL, glycosphingolipid; Hex, hexadecenal; LacCer, lactosylceramide; Spg, sphingosine. Data are means \pm SEMs, $n = 8$ WT and $n = 8$ BLAJ mice. * $P < 0.05$ versus WT as assessed by two-tailed unpaired t -test.

Fatty acid metabolism in *Dysf*-deficient myofibers and adipocytes

The accumulation of lipids within ectopic tissues such as skeletal muscle is often associated with increases in fatty acid sarcolemmal transport, reduced fatty acid oxidation, enhanced incorporation of fatty acids into complex lipids, or a combination of these factors (27, 28). Our study investigated skeletal muscle fatty acid metabolism in dysferlinopathies and found that fatty acid uptake tended to increase ($P = 0.09$) and esterification into TG was increased by ~ 2 -fold in the soleus muscle of BLAJ mice. The changes in TG synthesis were accompanied by a marked increase in *Dgat2*, the terminal rate-limiting enzyme for TG synthesis. There was also a significant reduction in *Pnpla2*, which encodes ATGL, the rate-limiting enzyme for TG breakdown (29), and an increase in *Plin5* in BLAJ compared with WT mice, which would predict increased TG storage in myofibers (30). Together, these changes in gene expression are consistent with the increased ^{14}C -fatty acid tracer-determined rate of fatty acid incorporation into muscle TG of BLAJ mice, which reflects the balance between storage and breakdown. Because the lipid droplets within *Dysf*-deficient myofibers seem to be a pronounced feature of slow oxidative myofibers rather than fast glycolytic myofibers (9), the soleus of mice that is composed predominantly of slow type 1 and IIa myofibers is of particular relevance because this is the most like human skeletal muscle (31). Our recent functional studies of muscles from older BLAJ compared with WT mice (aged 10 months) show a greater impact of dysferlin deficiency on soleus (slow) compared with extensor digitorum longus (fast) muscles, emphasizing the impor-

tance of myofiber type-specific responses in disease manifestation (32). Thus, our findings have strong implications for understanding the human dysferlinopathy condition. Indeed, MRI studies show that the soleus is one of the first muscles manifesting pathological changes (4).

It is noteworthy that there were no differences in TG content between BLAJ and WT mice in the quadriceps muscles, yet BLAJ mice clearly display an increased capacity for fatty acid esterification to TG in soleus muscles. This may reflect differences in lipid metabolism between the different muscles (i.e., the soleus is predominantly slow type 1 and IIa myofibers, whereas the larger quadriceps contains many fast myofibers) (33, 34), resulting from metabolic changes associated with the prevailing nutritional and/or endocrine state in vivo or from other alterations in lipid metabolism that could not be assessed in the model systems used herein. This might include the dynamic trafficking of fatty acids through the intramyocellular TG pool before their eventual oxidation or storage into other complex lipids (35). Indeed, an increase in DG and other lipids (e.g., sphingolipids) is consistent with the possibility of increased intramyocellular lipolysis in muscle.

Another major determinant of ectopic lipid deposition is fatty acid delivery to tissues. The importance of this mechanism is highlighted by studies in which intravenous infusion of a TG emulsion and heparin raises circulating NEFAs by ~ 3 - to 4-fold, which in turn increases intramyocellular lipids within 2 to 4 h (33, 34, 36). Our study demonstrates that adipose tissue lipolysis is increased in BLAJ mice under basal (i.e., spontaneous) conditions and in response to β -adrenergic stimulation. That plasma NEFAs and glycerol were not different between groups does not contradict these results because we have no in vivo assessment of the fatty acid rate of appearance or disappearance. Just how dysferlin deficiency influences lipolysis is unknown. Adipocyte lipolysis is regulated by the coordinate actions of the lipases ATGL, hormone-sensitive lipase, and monoglyceride lipase, which are generally located at the surface of lipid droplets within adipocytes. The activity of these lipases is regulated by posttranslational modifications, most notably activation by protein kinase A-mediated phosphorylation in serine sites but also complex interactions with several lipid-droplet associated effector proteins, including CGI-58, perilipin 1, and GOS2 (37). Dysferlin was previously identified as a lipid droplet-associated protein in the heart of rats, and the C2 domain was required for its lipid droplet localization (38). Hence, dysferlin may be required for orchestrating components of the molecular machinery that controls lipolysis, and this possibly will be the subject of future detailed investigations. Fatty acids can also be delivered to skeletal muscle via lipoprotein lipase-mediated cleavage of circulating TGs, but this is unlikely to be an additional source of excess NEFAs in BLAJ mice because TG secretion rates and plasma TG levels were similar in BLAJ and WT mice. Collectively, our data show that lipid accumulation associated with dysferlinopathies results from increased fatty acid delivery via increased adipose tissue lipolysis and the reprogramming of skeletal muscle fatty acid metabolism toward lipid storage.

Dysferlin deficiency affects the skeletal muscle lipidome

A major feature of dysferlinopathies is the marked accumulation of intramyocellular lipid droplets and apparent replacement of myofibers with adipocytes later in the pathology. By examining the skeletal muscle lipidome of young adult BLAJ mice, we have broadened the understanding of lipid changes in *Dysf*-deficient muscles independent of the confounding contamination by adipocytes. The lipidomic analysis revealed very different lipid profiles between BLAJ and WT mice, with significant increases in a broad array of lipids, including sphingolipids, phospholipids, lysophospholipids, cholesterol, and cholesteryl esters. It is well recognized that disturbances of sarcolemma properties and resealing are striking features of *Dysf*-deficient muscles (39), and experiments in *Dysf*-deficient mouse models indicate that high levels of cholesterol are deleterious to dysferlinopathic muscles (40). Of the extensive changes described in our lipidomic analysis, perhaps the most important findings are those that might affect the biophysical characteristics of the cell membrane. Phospholipids, sphingolipids, and cholesterol lipid species are all major components of the sarcolemma (41), and we report marked changes in many of these lipids in BLAJ mice, effects that were associated with altered expression of genes encoding regulatory proteins of sphingolipid and phospholipid metabolism. Decreases in the PC-PE ratio are associated with loss of membrane integrity in some cell types (42); however, this was not different between BLAJ and WT mice. Such altered lipid composition will affect many membrane properties, including biophysical properties such as fluidity that can influence vesicle trafficking and transmembrane transport (43, 44). Significantly, altered vesicle trafficking associated with sarcolemma resealing after experimental injury is a striking classic feature of *Dysf*-deficient muscles (11–13). *Dysf*-deficient muscles also show greater susceptibility to osmotic shock injury (45), with slower recovery to glycerol-induced osmotic shock (15), indicating altered sarcolemmal properties. There is good evidence that a primary defect in skeletal myofibers per se initiates the resultant pathology of dysferlinopathies (46). The consequences of altered lipid composition of membranes and metabolism are of wide interest to many skeletal and cardiac muscle disorders (43), and the current study should stimulate further investigation of dysferlinopathies.

Understanding the factors mediating skeletal muscle lipid accumulation has major clinical implications because both intra- and extramyocellular lipid accumulation is associated with insulin resistance (47) and other lipotoxic outcomes such as oxidative stress, activation of proinflammatory signaling, and induction of apoptotic signaling (43, 48). Such effects of lipids are highly relevant to dysferlinopathies, for which there is evidence of increased oxidative stress in *Dysf*-deficient human muscles (49) and in mouse muscles (23), where elevated lipofuscin in mice aged 3 months indicates that irreversible oxidative damage precedes overt histopathology. Ceramides function in a topographically restricted manner to regulate many cell processes, including apoptosis, senescence, signaling from

membrane receptors, and insulin signal transduction, and their accumulation in skeletal muscle is associated with several disease states, including type 2 diabetes (50). In this regard, while total ceramide levels were not increased in BLAJ muscles, there were significant increases in several species, most notably ceramide C16:0, which has been implicated in insulin resistance development in mice and humans (51, 52). Interestingly, this finding is inconsistent with the dominant expression of ceramide synthase 1 in muscles, which produces ceramide with a C18:0 acyl chain, and other studies reporting a ceramide C18:0 signature for insulin resistance in humans (53), but it is consistent with a likely increase in C16:0 substrate. Other complex sphingolipids such as glycosphingolipids (54) and dihydroceramide are implicated in insulin resistance, as are DGs via the activation of protein kinase C ϵ and inhibition of insulin signal transduction. While these lipids were uniformly elevated in the muscles of BLAJ mice, there was no evidence of insulin resistance or glucose intolerance. Such a phenotype may develop in later-onset disease. Finally, the increase in glycosphingolipids is indicative of a lysosomal defect in BLAJ mice that is somewhat supported by previous studies showing that dysferlin determines lysosome fusion to the plasma membrane (55). In total, this lipidomic analysis provides new insights into the changes accompanying *Dysf* deficiency and paves the way for targeted subcellular and temporal lipidomics to better define the mechanisms underlying pathological lipid accumulation in dysferlinopathies.

Systemic metabolic implications of *Dysf* deficiency


These studies also identified other metabolic features of interest. In brief, BLAJ mice had increased physical activity, RER, and increased food intake, especially after fasting, indicative of altered systemic metabolism and altered substrate metabolism. The plasma insulin levels were markedly decreased in BLAJ mice, both with fasting and in response to an oral glucose load, suggesting a potential role for dysferlin in insulin secretion by pancreatic β -cells or increased clearance, presumably by the liver. This line of inquiry warrants further examination. We observed no differences in whole-body insulin sensitivity (intraperitoneal insulin tolerance test) or liver insulin action as determined by phosphorylation of proximal and distal proteins involved in insulin signal transduction, suggesting no effects of dysferlin deficiency on insulin action. We cannot, however, rule out effects in skeletal muscle or other organs. We further surmise that the maintenance of whole-body glycemic control despite reduced insulin levels may be mediated by improved glucose effectiveness in BLAJ mice (56).

We also analyzed livers to determine how widespread or consistent any metabolic consequences of dysferlin deficiency might be. Curiously, liver mass was increased in BLAJ compared with WT mice. This was not due to increased triglyceride or glycogen content in BLAJ mice, and while edema has been reported in *Dysf*-deficient human skeletal muscles (3) and may account for greater mass of soleus muscles from old BLAJ mice (32), this does not

explain the increase in liver mass in BLAJ mice. Thus, the reasons for the increase in liver mass remain unexplained. Finally, it is noted that genetic backgrounds of mice can lead to differences in their metabolic phenotype. Hence, it is possible that some changes observed in these studies might be attributable to small differences in genetic background because the control WT mice were not littermate controls of the BLAJ mice (i.e., not from heterozygous breeding): instead, the C57BL/6J WT mice and BLAJ mice (bred onto a pure C57BL/6J background) were maintained as separate colonies.

Human metabolism and dysferlinopathies

In the context of overall energy requirements, muscle metabolism, and substrate partitioning, it is relevant to consider how these may alter between normal growing muscles and the mature adult state because dysferlinopathy manifests in humans after puberty, usually within 1 to 2 years after the cessation of growth (24, 57). As fuel for energetic metabolism during exercise, children rely more on fat than carbohydrates compared with adults, and the transition to an adult-like metabolic profile occurs between middle to late puberty and is completed by the end of puberty (58, 59); such a metabolic shift from lipids to carbohydrates as fuels might contribute to the timing of the onset of disease manifestation of dysferlinopathies. The influence of gender on metabolism needs to be considered because there are profound effects of ovarian hormones on carbohydrate and fat metabolism and oxidative enzymes (58); such gender differences may contribute to the subsequent more severe fatty replacement of many muscles in female patients with dysferlinopathy (4). A study of normal male human myofiber type-specific development (size and satellite cell content) over the entire life-span (0–86 years) showed that during growth (0–18 years) there was a huge increase in myofiber size, with no major differences between type I (slow oxidative) and II (fast glycolytic) myofibers; however, postgrowth there was a selective atrophy of fast type 2 myofibers in adults that was pronounced with age and had metabolic implications (60). Likewise, in normal soleus and EDL muscles of adult male rats aged 3–12 months, there are substantial changes in many physiological and biochemical characteristics during early and middle adulthood (61). Thus, the impact of metabolic changes in dysferlinopathy on disease onset and progression also needs to be considered in the wider context of growth/age, gender, and myofiber type.

In conclusion, these novel results using presymptomatic young adult BLAJ mice highlight the central role for disturbances in skeletal muscle and adipose tissue lipid metabolism as an intrinsic, early manifestation that results from *Dysf* deficiency, with long-term adverse consequences for progressive disease severity with myofibers replaced by adipocytes and loss of function. This new focus on metabolism has many clinical implications and warrants further investigation. 

The authors thank Jaquelyn Weir and Natalie Mellett for technical support with the lipidomic analysis.

REFERENCES

- Bashir, R., S. Britton, T. Strachan, S. Keers, E. Vafiadaki, M. Lako, I. Richard, S. Marchand, N. Bourg, Z. Argov, et al. 1998. A gene related to *Caenorhabditis elegans* spermatogenesis factor *fer-1* is mutated in limb-girdle muscular dystrophy type 2B. *Nat. Genet.* **20**: 37–42.
- Harris, E., C. L. Bladen, A. Mayhew, M. James, K. Bettinson, U. Moore, F. E. Smith, L. Rufibach, A. Cnaan, D. X. Bharucha-Goebel, et al. 2016. The Clinical Outcome Study for dysferlinopathy: an international multicenter study. *Neurol. Genet.* **2**: e89.
- Fanin, M., and C. Angelini. 2016. Progress and challenges in diagnosis of dysferlinopathy. *Muscle Nerve.* **54**: 821–835.
- Diaz-Manera, J., R. Fernandez-Torron, J. LLauger, M. K. James, A. Mayhew, F. E. Smith, U. R. Moore, A. M. Blamire, P. G. Carlier, L. Rufibach, et al. 2018. Muscle MRI in patients with dysferlinopathy: pattern recognition and implications for clinical trials. *J. Neurol. Neurosurg. Psychiatry.* **89**: 1071–1081.
- Ho, M., C. M. Post, L. R. Donahue, H. G. W. Lidov, R. T. Bronson, H. Goolsby, S. C. Watkins, G. A. Cox, and R. H. Brown. 2004. Disruption of muscle membrane and phenotype divergence in two novel mouse models of dysferlin deficiency. *Hum. Mol. Genet.* **13**: 1999–2010.
- Hornsey, M. A., S. H. Laval, R. Barresi, H. Lochmuller, and K. Bushby. 2013. Muscular dystrophy in dysferlin-deficient mouse models. *Neuromuscul. Disord.* **23**: 377–387.
- Kobayashi, K., T. Izawa, M. Kuwamura, and J. Yamate. 2010. The distribution and characterization of skeletal muscle lesions in dysferlin-deficient SJL and A/J mice. *Exp. Toxicol. Pathol.* **62**: 509–517.
- Kobayashi, K., T. Izawa, M. Kuwamura, and J. Yamate. 2012. Dysferlin and animal models for dysferlinopathy. *J. Toxicol. Pathol.* **25**: 135–147.
- Grounds, M. D., J. R. Terrill, H. G. Radley-Crabb, T. Robertson, J. Papadimitriou, S. Spuler, and T. Shavlakadze. 2014. Lipid accumulation in dysferlin-deficient muscles. *Am. J. Pathol.* **184**: 1668–1676.
- Lek, A., F. J. Evesson, R. B. Sutton, K. N. North, and S. T. Cooper. 2012. Ferlins: regulators of vesicle fusion for auditory neurotransmission, receptor trafficking and membrane repair. *Traffic.* **13**: 185–194.
- Bansal, D., K. Miyake, S. S. Vogel, S. Groh, C. C. Chen, R. Williamson, P. L. McNeil, and K. P. Campbell. 2003. Defective membrane repair in dysferlin-deficient muscular dystrophy. *Nature.* **423**: 168–172.
- Glover, L., and R. H. Brown, Jr. 2007. Dysferlin in membrane trafficking and patch repair. *Traffic.* **8**: 785–794.
- Han, R., and K. P. Campbell. 2007. Dysferlin and muscle membrane repair. *Curr. Opin. Cell Biol.* **19**: 409–416.
- Al-Qusairi, L., and J. Laporte. 2011. T-tubule biogenesis and triad formation in skeletal muscle and implication in human diseases. *Skelet. Muscle.* **1**: 26.
- Demonbreun, A. R., A. E. Rossi, M. G. Alvarez, K. E. Swanson, H. K. Deveaux, J. U. Earley, M. Hadhazy, R. Vohra, G. A. Walter, P. Pytel, et al. 2014. Dysferlin and myoferlin regulate transverse tubule formation and glycerol sensitivity. *Am. J. Pathol.* **184**: 248–259.
- Klinge, L., J. Harris, C. Sewry, R. Charlton, L. Anderson, S. Laval, Y. H. Chiu, M. Hornsey, V. Straub, R. Barresi, et al. 2010. Dysferlin associates with the developing T-tubule system in rodent and human skeletal muscle. *Muscle Nerve.* **41**: 166–173.
- Roche, J. A., L. W. Ru, A. M. O'Neill, W. G. Resneck, R. M. Lovering, and R. J. Bloch. 2011. Unmasking potential intracellular roles for dysferlin through improved immunolabeling methods. *J. Histochem. Cytochem.* **59**: 964–975.
- Waddell, L. B., F. A. Lemckert, X. F. Zheng, J. Tran, F. J. Evesson, J. M. Hawkes, A. Lek, N. E. Street, P. Lin, N. F. Clarke, et al. 2011. Dysferlin, annexin A1, and mitsugumin 53 are upregulated in muscular dystrophy and localize to longitudinal tubules of the T-system with stretch. *J. Neuropathol. Exp. Neurol.* **70**: 302–313.
- Anderson, L. V., K. Davison, J. A. Moss, C. Young, M. J. Cullen, J. Walsh, M. A. Johnson, R. Bashir, S. Britton, S. Keers, et al. 1999. Dysferlin is a plasma membrane protein and is expressed early in human development. *Hum. Mol. Genet.* **8**: 855–861.
- Prior, M. J., M. Larance, R. T. Lawrence, J. Soul, S. Humphrey, J. Burchfield, C. Kistler, J. R. Davey, P. J. La-Borde, M. Buckley, et al. 2011. Quantitative proteomic analysis of the adipocyte plasma membrane. *J. Proteome Res.* **10**: 4970–4982.
- Nagaraju, K., R. Rawat, E. Veszelszky, R. Thapliyal, A. Kesari, S. Sparks, N. Raben, P. Plotz, and E. P. Hoffman. 2008. Dysferlin

- deficiency enhances monocyte phagocytosis: a model for the inflammatory onset of limb-girdle muscular dystrophy 2B. *Am. J. Pathol.* **172**: 774–785.
22. Sharma, A., C. Yu, C. Leung, A. Trane, M. Lau, S. Utokaparch, F. Shaheen, N. Sheibani, and P. Bernatchez. 2010. A new role for the muscle repair protein dysferlin in endothelial cell adhesion and angiogenesis. *Arterioscler. Thromb. Vasc. Biol.* **30**: 2196–2204.
 23. Terrill, J. R., H. G. Radley-Crabb, T. Iwasaki, F. A. Lemckert, P. G. Arthur, and M. D. Grounds. 2013. Oxidative stress and pathology in muscular dystrophies: focus on protein thiol oxidation and dysferlinopathies. *FEBS J.* **280**: 4149–4164.
 24. Angelini, C., E. Peterle, A. Gaiani, L. Bortolussi, and C. Borsato. 2011. Dysferlinopathy course and sportive activity: clues for possible treatment. *Acta Myol.* **30**: 127–132.
 25. Fanin, M., A. C. Nascimbeni, and C. Angelini. 2014. Muscle atrophy, ubiquitin-proteasome, and autophagic pathways in dysferlinopathy. *Muscle Nerve.* **50**: 340–347.
 26. Cenacchi, G., M. Fanin, L. B. De Giorgi, and C. Angelini. 2005. Ultrastructural changes in dysferlinopathy support defective membrane repair mechanism. *J. Clin. Pathol.* **58**: 190–195.
 27. Glatz, J. F. C., and J. Luiken. 2018. Dynamic role of the transmembrane glycoprotein CD36 (SR-B2) in cellular fatty acid uptake and utilization. *J. Lipid Res.* **59**: 1084–1093.
 28. Goodpaster, B. H., and L. M. Sparks. 2017. Metabolic flexibility in health and disease. *Cell Metab.* **25**: 1027–1036.
 29. Zimmermann, R., J. G. Strauss, G. Haemmerle, G. Schoiswohl, R. Birner-Gruenberger, M. Riederer, A. Lass, G. Neuberger, F. Eisenhaber, A. Hermetter, et al. 2004. Fat mobilization in adipose tissue is promoted by adipose triglyceride lipase. *Science.* **306**: 1383–1386.
 30. Mason, R. R., and M. J. Watt. 2015. Unraveling the roles of PLIN5: linking cell biology to physiology. *Trends Endocrinol. Metab.* **26**: 144–152.
 31. Kho, A. T., P. B. Kang, I. S. Kohane, and L. M. Kunkel. 2006. Transcriptome-scale similarities between mouse and human skeletal muscles with normal and myopathic phenotypes. *BMC Musculoskelet. Disord.* **7**: 23.
 32. Lloyd, E. M., H. Xu, R. M. Murphy, M. D. Grounds, and G. J. Pinniger. 2019. Dysferlin-deficiency has greater impact on function of slow muscles, compared with fast, in aged BLA/J mice. *PLoS One.* **14**: e0214908.
 33. Yu, C., Y. Chen, G. W. Cline, D. Zhang, H. Zong, Y. Wang, R. Bergeron, J. K. Kim, S. W. Cushman, G. J. Cooney, et al. 2002. Mechanism by which fatty acids inhibit insulin activation of insulin receptor substrate-1 (IRS-1)-associated phosphatidylinositol 3-kinase activity in muscle. *J. Biol. Chem.* **277**: 50230–50236.
 34. Boden, G., B. Lebed, M. Schatz, C. Homko, and S. Lemieux. 2001. Effects of acute changes of plasma free fatty acids on intramyocellular fat content and insulin resistance in healthy subjects. *Diabetes.* **50**: 1612–1617.
 35. Meex, R. C., A. J. Hoy, R. M. Mason, S. D. Martin, S. L. McGee, C. R. Bruce, and M. J. Watt. 2015. ATGL-mediated triglyceride turnover and the regulation of mitochondrial capacity in skeletal muscle. *Am. J. Physiol. Endocrinol. Metab.* **308**: E960–E970.
 36. Watt, M. J., A. Hevener, G. I. Lancaster, and M. A. Febbraio. 2006. Ciliary neurotrophic factor prevents acute lipid-induced insulin resistance by attenuating ceramide accumulation and phosphorylation of c-Jun N-terminal kinase in peripheral tissues. *Endocrinology.* **147**: 2077–2085.
 37. Raajendiran, A., T. Tsiloulis, and M. J. Watt. 2016. Adipose tissue development and the molecular regulation of lipid metabolism. *Essays Biochem.* **60**: 437–450.
 38. Li, L., H. N. Zhang, W. Y. Wang, Y. Hong, J. F. Wang, S. Y. Zhang, S. M. Xu, Q. B. Shu, J. F. Li, F. Q. Yang, et al. 2016. Comparative proteomics reveals abnormal binding of ATGL and dysferlin on lipid droplets from pressure overload-induced dysfunctional rat hearts. *Sci Rep.* **6**: 19782.
 39. Demonbreun, A. R., M. V. Allen, J. L. Warner, D. Y. Barefield, S. Krishnan, K. E. Swanson, J. U. Earley, and E. M. McNally. 2016. Enhanced muscular dystrophy from loss of dysferlin is accompanied by impaired annexin A6 translocation after sarcolemmal disruption. *Am. J. Pathol.* **186**: 1610–1622.
 40. Sellers, S. L., N. Milad, Z. White, C. Pascoe, R. Chan, G. W. Payne, C. Seow, F. Rossi, M. A. Seidman, and P. Bernatchez. 2018. Increased nonHDL cholesterol levels cause muscle wasting and ambulatory dysfunction in the mouse model of LGMD2B. *J. Lipid Res.* **59**: 261–272.
 41. Fiehn, W., J. B. Peter, J. F. Mead, and M. Gan-Elepano. 1971. Lipids and fatty acids of sarcolemma, sarcoplasmic reticulum, and mitochondria from rat skeletal muscle. *J. Biol. Chem.* **246**: 5617–5620.
 42. Li, Z., L. B. Agellon, T. M. Allen, M. Umeda, L. Jewell, A. Mason, and D. E. Vance. 2006. The ratio of phosphatidylcholine to phosphatidylethanolamine influences membrane integrity and steatohepatitis. *Cell Metab.* **3**: 321–331.
 43. Saini-Chohan, H. K., R. W. Mitchell, F. M. Vaz, T. Zelinski, and G. M. Hatch. 2012. Delineating the role of alterations in lipid metabolism in the pathogenesis of inherited skeletal and cardiac muscle disorders: Thematic Review Series: Genetics of Human Lipid Diseases. *J. Lipid Res.* **53**: 4–27.
 44. Spector, A. A., and M. A. Yorek. 1985. Membrane lipid composition and cellular function. *J. Lipid Res.* **26**: 1015–1035.
 45. Lukyanenko, V., J. M. Muriel, and R. J. Bloch. 2017. Coupling of excitation to Ca²⁺ release is modulated by dysferlin. *J. Physiol.* **595**: 5191–5207.
 46. Millay, D. P., M. Maillet, J. A. Roche, M. A. Sargent, E. M. McNally, R. J. Bloch, and J. D. Molkentin. 2009. Genetic manipulation of dysferlin expression in skeletal muscle: novel insights into muscular dystrophy. *Am. J. Pathol.* **175**: 1817–1823.
 47. Sinha, R., S. Dufour, K. F. Petersen, V. LeBon, S. Enoksson, Y. Z. Ma, M. Savoye, D. L. Rothman, G. I. Shulman, and S. Caprio. 2002. Assessment of skeletal muscle triglyceride content by H-1 nuclear magnetic resonance spectroscopy in lean and obese adolescents: relationships to insulin sensitivity, total body fat, and central adiposity. *Diabetes.* **51**: 1022–1027.
 48. Bonnard, C., A. Durand, S. Peyrol, E. Chanseaux, M. A. Chauvin, B. Morio, H. Vidal, and J. Rieusset. 2008. Mitochondrial dysfunction results from oxidative stress in the skeletal muscle of diet-induced insulin-resistant mice. *J. Clin. Invest.* **118**: 789–800.
 49. Rajakumar, D., S. Senguttuvan, M. Alexander, and A. Oommen. 2014. Involvement of oxidative stress, nuclear factor kappa B and the ubiquitin proteasomal pathway in dysferlinopathy. *Life Sci.* **108**: 54–61.
 50. Chaurasia, B., and S. A. Summers. 2015. Ceramides - lipotoxic inducers of metabolic disorders. *Trends Endocrinol. Metab.* **26**: 538–550.
 51. Turpin, S. M., H. T. Nicholls, D. M. Willmes, A. Mourier, S. Brodesser, C. M. Wunderlich, J. Mauer, E. Xu, P. Hammerschmidt, H. S. Bronneke, et al. 2014. Obesity-induced CerS6-dependent C16:0 ceramide production promotes weight gain and glucose intolerance. *Cell Metab.* **20**: 678–686.
 52. Adams 2nd, J. M., T. Pratipanawat, R. Berria, E. Wang, R. A. DeFronzo, M. C. Sullards, and L. J. Mandarino. 2004. Ceramide content is increased in skeletal muscle from obese insulin-resistant humans. *Diabetes.* **53**: 25–31.
 53. Bergman, B. C., J. T. Brozinick, A. Strauss, S. Bacon, A. Kerege, H. H. Bui, P. Sanders, P. Siddall, T. Wei, M. K. Thomas, et al. 2016. Muscle sphingolipids during rest and exercise: a C18:0 signature for insulin resistance in humans. *Diabetologia.* **59**: 785–798.
 54. Aerts, J. M., R. G. Boot, M. van Eijk, J. Groener, N. Bijl, E. Lombardo, F. M. Bietrix, N. Dekker, A. K. Groen, R. Ottenhoff, et al. 2011. Glycosphingolipids and insulin resistance. *Adv. Exp. Med. Biol.* **721**: 99–119.
 55. Han, W. Q., M. Xia, M. Xu, K. M. Boini, J. K. Ritter, N. J. Li, and P. L. Li. 2012. Lysosome fusion to the cell membrane is mediated by the dysferlin C2A domain in coronary arterial endothelial cells. *J. Cell Sci.* **125**: 1225–1234.
 56. Best, J. D., S. E. Kahn, M. Ader, R. M. Watanabe, T. C. Ni, and R. N. Bergman. 1996. Role of glucose effectiveness in the determination of glucose tolerance. *Diabetes Care.* **19**: 1018–1030.
 57. Albrecht, D. E., N. Garg, L. E. Rufibach, B. A. Williams, N. Monnier, E. Hwang, and P. Mittal. 2011. 4th Annual Dysferlin Conference 11–14 September 2010, Washington, USA. *Neuromuscul. Disord.* **21**: 304–310.
 58. Aucouturier, J., J. S. Baker, and P. Duche. 2008. Fat and carbohydrate metabolism during submaximal exercise in children. *Sports Med.* **38**: 213–238.
 59. Stephens, B. R., A. S. Cole, and A. D. Mahon. 2006. The influence of biological maturation on fat and carbohydrate metabolism during exercise in males. *Int. J. Sport Nutr. Exerc. Metab.* **16**: 166–179.
 60. Verdijk, L. B., T. Snijders, M. Drost, T. Delhaas, F. Kadi, and L. J. van Loon. 2014. Satellite cells in human skeletal muscle; from birth to old age. *Age (Dordr.)* **36**: 545–547.
 61. Xu, H., G. D. Lamb, and R. M. Murphy. 2017. Changes in contractile and metabolic parameters of skeletal muscle as rats age from 3 to 12 months. *J. Muscle Res. Cell Motil.* **38**: 405–420.